Effect of Incident Laser Sheet Orientation on the OH-PLIF Imaging of Detonations

K.P. Chatelain[1], R. Mével[2,3], J. Melguizo-Gavilanes[4], A. Chinnayya[4], S. Xu[5], D.A. Lacoste[1]

[1] King Abdullah University of Science and Technology (KAUST), Clean Combustion Research Center (CCRC), Thuwal, Saudi Arabia

[2] Center for Combustion Energy, Tsinghua University, Beijing, China

[3] Department of Automotive Engineering, Tsinghua University, Beijing, China

[4] Institut Pprime, UPR 3346 CNRS, ISAE-ENSMA, Futuroscope-Chasseneuil Cedex, France

[5] School of Aerospace Engineering, Tsinghua University, Beijing, China

1 Introduction

Planar Laser-Induced Fluorescence of OH radical (OH-PLIF) is a common technique used to characterize the geometry of the reaction zone in weakly [1,2] and highly unstable detonations [3]. To enable direct comparison between the experimental PLIF images and 2-D numerical simulations, Mével et al. [4] developed a LIF model to obtain numerical PLIF images. They showed that the PLIF images are less and less representative of the OH fields as the distance behind the shock front increases. Indeed under detonation conditions, the LIF process is within the optically-thick regime. In other words, the strong absorption of incident laser light by the high OH concentration at the beginning of the reaction zone makes the zones of high concentration of OH away from the front less visible due to the attenuation of the laser light as it travels through the medium. Mével et al. [4] focused on a single laser configuration for which the incident light is traveling opposite to the detonation wave. However, other recent studies [5–7] employed a different experimental configuration in which the laser light propagates perpendicular to the direction of detonation propagation. Such a configuration might enable to observe regions of high OH-concentration located far downstream of the detonation front. The goal of the present study is to investigate the effect of the incident laser light sheet orientation on the OH-PLIF imaging of the reaction zone of detonation waves. For the purpose of this contribution, we limited our investigation to a weakly unstable detonation propagating in hydrogen-oxygen mixtures highly diluted with argon to enable direct comparison with the experimental OH-PLIF images available in the literature. An updated LIF model has been developed and validated using steady one-dimensional (1-D) and unsteady two-dimensional (2-D) numerical simulations. A comparison of two numerical OH-PLIF images obtained with the aforementioned laser orientations is performed to highlight the advantages and drawbacks of the two configurations.

2 Numerical simulation methods

2.1 Laser induced fluorescence model

Similarly to Mével et al. [4], we employed the 3-level LIF model of Besslet et al. [8]. In the linear regime and at steady-state, the fluorescence intensity for one pumped electronic transition is given by Equation 1,

$$F \propto f_B \Gamma I_\nu^0 I_b N_{OH} B \frac{1}{Q} \sum A_i, \tag{1}$$

where f_B is the Boltzmann fraction, Γ is the dimensionless overlap integral, I_ν^0 is the normalized spectral laser irradiance, I_b is a dimensionless factor accounting for the light sheet absorption, N_{OH} is the OH radical number density, B is the Einstein B coefficient, Q is the quenching rate, and A_i are the Einstein A coefficients.

Correspondence to: karl.chatelain@kaust.edu.sa

The parameters in Equation 1 are calculated as described in Mével et al. [4] with five main changes: (i) different optical paths can now be considered due to the possible laser orientations with respect to the detonation front; (ii) the collisional broadening ($\Delta\nu_c$) is calculated more accurately using Equation 2,

$$\Delta\nu_c = P\sum_A X_A\sigma_{AB}^2\left(\frac{8}{\pi\mu_{AB}kT}\right)^{\frac{1}{2}} \tag{2}$$

where P is the pressure, T is the temperature, k is the Boltzmann's constant, X_A is the mole fraction of species A, and σ_{AB} and μ_{AB} correspond, respectively, to the optical collision diameter and the reduced mass between any species A in the gas mixture with the fluorescent species ($B = OH$); (iii) the absorption lineshape function is calculated using a Voigt profile as described in [9]; (iv) the pressure line-center shift of the transition lines is calculated for both laser orientations and is obtained with Equation 3 [9, 10],

$$\nu_{\text{shifted}} = \nu_0 + P\sum_A X_A\delta_{A,T_{\text{ref}}}\left(T_{\text{ref}}/T\right)^M \tag{3}$$

where ν_0 and ν_{shifted} correspond, respectively, to the initial and the shifted transition center-line, $\delta_{A,T_{\text{ref}}}$ and M are the pressure shift parameters associated to a given species (A) at a reference temperature (T_{ref}). The Doppler line-shift is neglected due to its expected low contribution (<1 pm) in the present conditions; (v) five transitions are employed ($P_1(5)$, $Q_{21}(9)$, $Q_2(8)$, $Q_1(9)$, $Q_{12}(8)$ (shown as dashed lines in Figure 1) whereas Mével et al. [4] used only $Q_2(8)$, $Q_1(9)$. This more complex approach is justified by the higher initial pressure used by Wang et al. [7] than that of Austin et al. [3]. The contribution of the adjacent absorption lines is illustrated in Figure 1 for conditions corresponding to the von Neumann and the Chapman-Jouguet (CJ) states.

The dimensions of the laser sheet and the Gaussian spatial distribution of the laser energy [11] are taken into account to accurately compare the experimental and simulated LIF signals for each validation case. Additionally, the curvature of the detonation front is accounted for the non-homogeneous optical path in the 1-D simulations (ZND). It is considered by displacing the detonation front in the ZND calculation by the offset observed in the experimental PLIF images. This correction is not applied on the 2-D simulations.

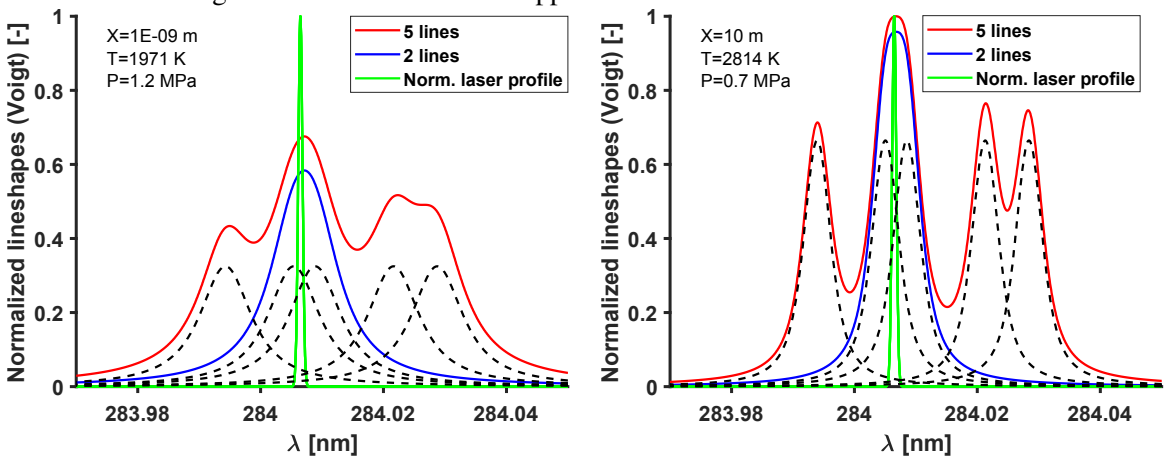

a) von Neumann state b) CJ state

Figure 1: Effect of the number of absorption lines considered to calculate the transition lineshapes at two positions (X) relative to the detonation front. The normalization is performed considering the maximum over the entire ZND profile. Conditions: $2H_2$-O_2-10Ar at P_1 = 45.3 kPa and T_1 = 295 K.

2.2 Reaction model

The reaction model employed for all the simulations is the reaction model of Mével et al. [12]. It is composed of 9 chemical species (including Ar) and 29 reversible reactions. It has been extensively validated and has

demonstrated good predictive capabilities [13].

2.3 Detonation models

The steady 1-D detonation simulations were performed using a ZND code implemented in CHEMKIN-II. It is based on the work of Shepherd [14] and is equivalent to the ZND code available within the Shock and Detonation Toolbox implemented with Cantera [15].

The unsteady 2-D simulations were performed using an inviscid formulation with detailed chemistry. Particulars about the numerical methods used, spatial and temporal discretizations as well as the parallelization methodology can be found in [16]. Briefly, we used time-operator splitting to couple the hydrodynamics to the chemistry together with directional splitting, along with a ninth-order monotonicity preserving interpolation in space, and a third order explicit Runge-Kutta in time. For the integration of the chemical source terms and to avoid being limited by the smallest time scales dictated by the chemistry, we implemented the methodology described in [17] to approximate the diagonal of the chemical Jacobian. Although this method was proposed in the context of turbulent flames simulations, it seems to perform efficiently in detonation flows as well. Simulations were run in the laboratory frame of reference using 400 processors and a fixed squared domain of side 40 mm. A sliding window technique was used to keep the propagating detonation within the computational domain at all times.

2.4 Validation methodology

To compare the experimental results with the steady 1-D simulations, it was required to extract 1-D LIF intensity profiles from the PLIF images. The post-processing sequence is illustrated in Figure 2 and comprises: (i) define arbitrary subdomains of interest; (ii) normalize the profile in this subdomain; (iii) perform a vertical averaging of the signal to get the 1-D profile. The 2-D validation of the model relies on a comparison of the experimental images and a 2-D synthetic PLIF image following the methodology described in Mével et al. [4].

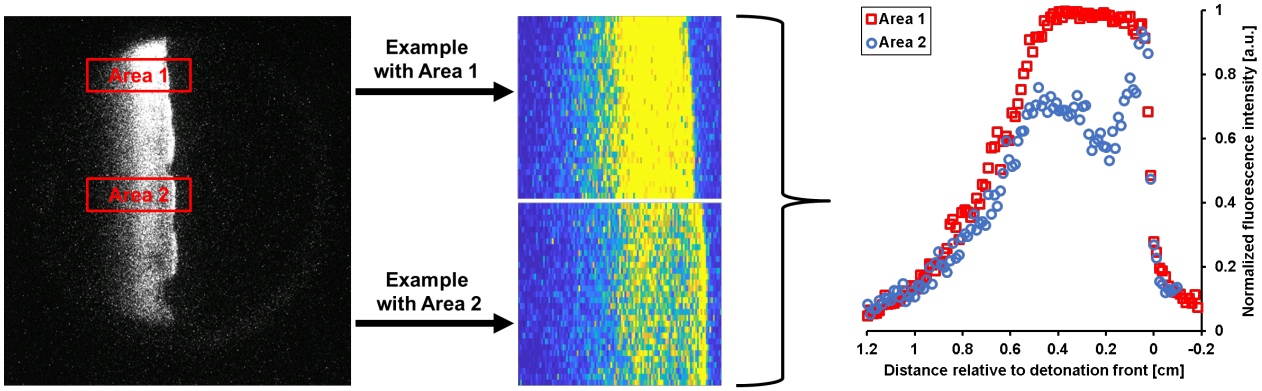

Figure 2: Post-processing methodology: extraction of 1-D LIF intensity profiles from the experimental PLIF images. Conditions: $2H_2$-O_2-10Ar at P_1 = 45.3 kPa and T_1 = 295 K.

3 Results and discussion

3.1 Validation using steady 1-D simulation

Head-on laser orientation Figure 3 presents two validation cases of the present LIF model with a head-on laser orientation from Austin [1]. The present LIF model reproduces the experimental 1-D profiles for all the area investigated. From this comparison and the results obtained with other areas not presented here, it can be concluded that the modifications made to the LIF model did not degrade the overall agreement between the experimental and calculated profiles for the head-on configuration.

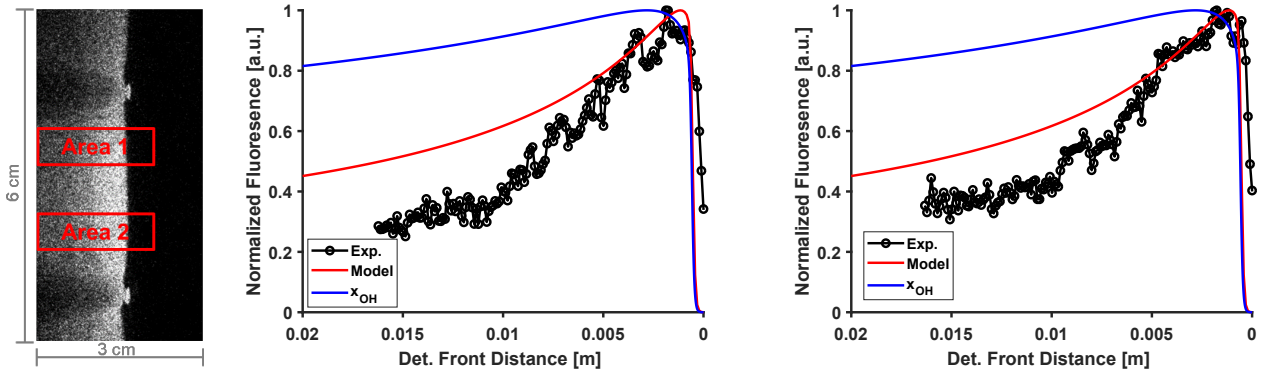

a) Exp. PLIF b) Validation on area 1 c) Validation on area 2

Figure 3: Experimental [1] and ZND 1-D LIF profiles obtained for a head-on laser orientation, respectively in black and red lines. ZND OH mole fractions (blue lines) are represented for comparison. Conditions: $2H_2$-O_2-12Ar at P_1=20 kPa and T_1=295 K.

Transverse laser orientation Figure 4 shows a comparison between the experimental (Wang's data [7]) and simulated 1-D LIF profiles for two different areas along the vertical axis.
A few things are noteworthy, first, the 1-D LIF signal obtained with the transverse laser orientation is not representative of the X_{OH} profile and the LIF signal decreases rapidly after the detonation front, similar to the head-on configuration. This decrease seems induced by the experimental setup, that uses a relatively narrow laser sheet (24 mm) for which only half of the sheet illuminates the reaction front. The other half of the sheet shines on the fresh gases located ahead of the detonation front.

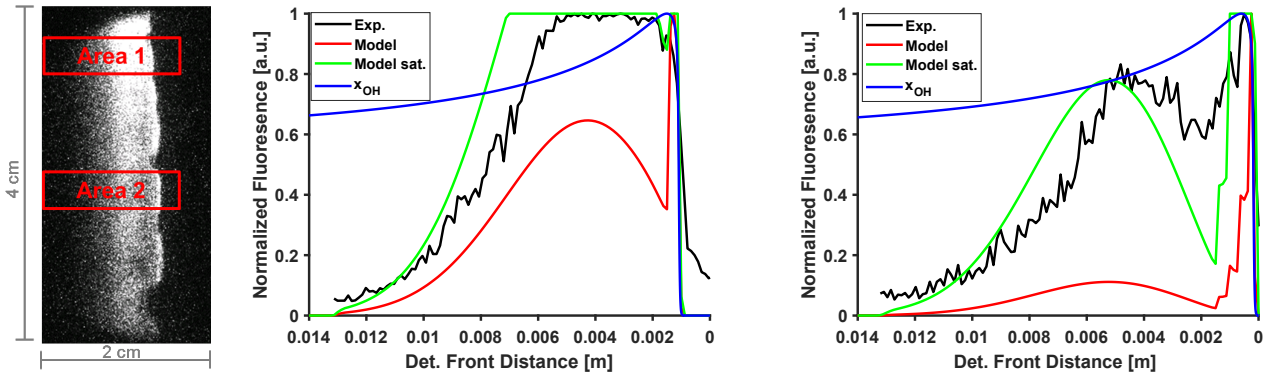

a) Exp. PLIF b) Validation on area 1 c) Validation on area 2

Figure 4: Experimental [7] (black lines) and ZND 1-D (red and green lines) LIF profiles obtained for a transverse laser orientation. ZND OH mole fractions (blue lines) are represented for comparison. Conditions: $2H_2$-O_2-10Ar at P_1 = 45.3 kPa and T_1 = 295 K.

Second, the base numerical LIF signal (referred to as Model in Figures 4 b) and c)) reproduces the decrease of the experimental signal but not the overall shape. These results already consider (i) the non-homogeneous optical path, (ii) the spatial distribution of the laser energy and (iii) the curvature of the detonation front, but do not consider the saturation on the experimental images. To improve the agreement, this saturation was simulated (referred to as Model sat.) by amplifying the LIF signal and clipping the maximum value to 1. The agreement between the experimental and the modeled LIF signals (Figures 4 b) and c)) is significantly improved

by accounting for the saturation. Similar agreement is obtained for several areas located at different heights of the detonation.

Many aspects of the imaging system had to be included to obtain a qualitative agreement with the experimental data. To the best of our knowledge, all the images currently available in the literature [5, 6] with the transverse laser orientation show some degree of saturation hence no further validation can be performed. Since some of these aspects are difficult to quantify in the present validation data, additional experimental data are required to better validate the model. These new experimental data must be obtained with OH-PLIF images free of saturation and with a known spatial distribution of the incident laser energy.

3.2 Unsteady 2-D simulation

Experimental-numerical comparison of the 2-D PLIF signals As shown in Figures 5 a) and b), there are significant differences between the curved and saturated experimental PLIF fields and the ideal, essentially flat numerical one. The use of the LIF model on the 2-D fields evidenced a strong absorption of the laser energy along the vertical axis. In Figure 5 b), the numerical LIF signal rapidly drops close to 0 after only 2 cm. The double peaks observed experimentally, which were reproduced with the 1-D simulations (Figure 4), are also observed on the 2-D numerical PLIF (see line at 3.3 mm inn Figure 5 c)). In addition, even more complex profiles can be observed for different vertical positions (see line at 9.9 mm in Figure 5 c)). These are due to the combination of the OH concentration fluctuations and the spatial distribution of the laser energy inside the reaction front. These very complex LIF intensity profiles emphasize the need for new experimental data with precise measurements of the laser energy profile to fully validate the vertical orientation of the LIF model.

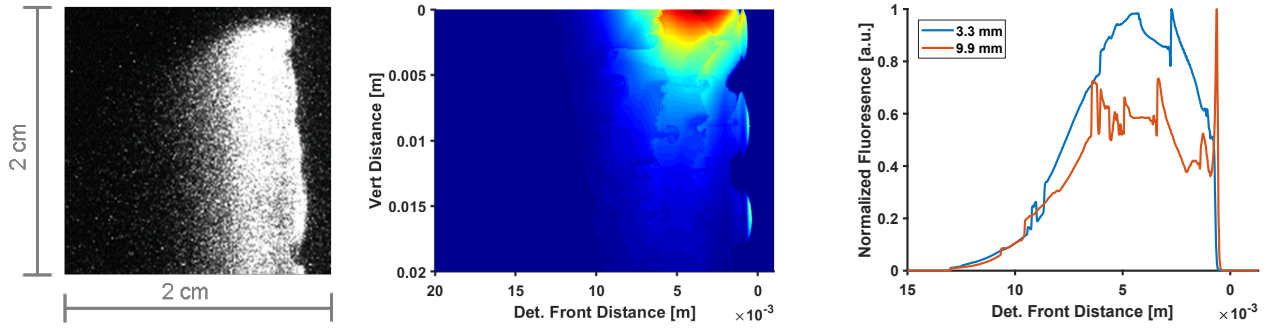

a) Experimental OH-PLIF b) Numerical OH-PLIF c) Numerical 1-D OH-LIF signals

Figure 5: Comparison between the experimental and numerical OH-PLIF images. (a) experiment; (b) simulation; (c) normalized 1-D LIF profiles at two different heights. Conditions: $2H_2$-O_2-10Ar at P_1 = 45.3 kPa and T_1 = 295 K.

Effects of the laser orientation on an ideal detonation front The effect of the two laser orientations is investigated using the results from the unsteady 2-D simulation, see Figure 6. These results consider an ideal laser sheet (without a Gaussian spatial energy distribution) to pleclude the effect of the laser energy profile which was not measured experimentally. For a head-on configuration, the present results are similar to those obtained by Mével et al. [4] with a high fluorescence intensity confined at the detonation front. The use of a transverse laser orientation enables to visualize regions of high LIF intensity (see Figure 6 c)) far behind the detonation front and about 1 cm into the field vertically. In the case of the transverse laser orientation, the LIF intensity (at least for short optical paths) better represents the OH profile along the detonation front compared to the head-on laser orientation. In addition, the LIF signal obtained with the transverse laser orientation enables to observe, to some extent, the patterns generated by the OH concentration gradients in Figure 6 a) but with different intensities. Both observations are not possible with the head-on laser orientation due to the optical thickness of the detonation front.

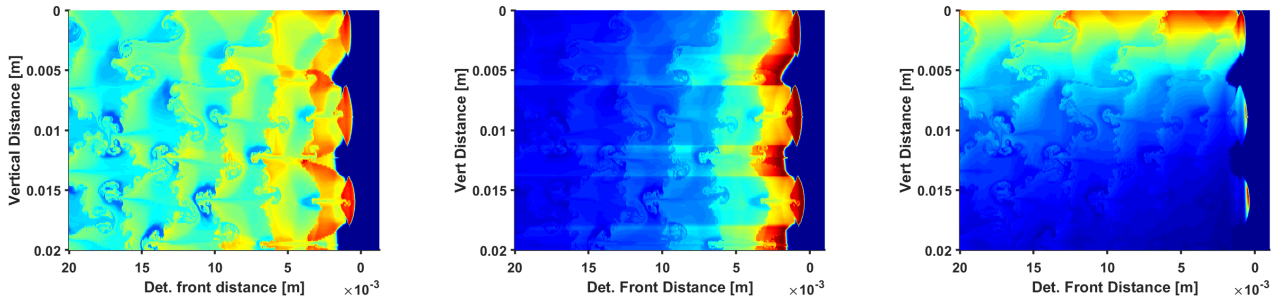

a) 2-D field of OH b) Head-on laser orientation c) Transverse laser orientation

Figure 6: Modeled OH-PLIF images with different laser orientations in b) and c). The numerical 2-D field of OH is given in a) for comparison. Conditions: $2H_2$-O_2-10Ar at P_1 = 45.3 kPa and T_1 = 295 K.

4 Conclusion

The vertical orientation of the incident laser sheet in the PLIF imaging system might enable to observe regions of high OH-concentration behind the detonation front. While the visualization of domains with relatively short optical paths enables such observation, domains far from it are significantly affected by laser absorption because a detonation is an optically-thick reactive flow. In addition, the curvature of the detonation front can create a non-homogeneous optical path which complicates the interpretation of the PLIF images and LIF profiles extracted from them. Such an effect is not observed for the PLIF imaging with the head-on laser light orientation. The present work demonstrates that the use of the transverse laser orientation with (i) a wide laser sheet and (ii) a known and appropriate spatial distribution of the laser energy allows to visualize reactive areas behind the detonation front. While these first results show a qualitative agreement with experimental data, bear in mind that the transverse laser orientation of the LIF model is not fully validated yet. New experimental data are required to validate the transverse laser orientation of the LIF model and to conclusively confirm whether this laser orientation provides useful additional information during visualization of the detonation front.

References

[1] Austin J. (2003). Ph.D. thesis, California Institute of Technology.
[2] Pintgen F. (2000). Master's thesis, Technische Universität München and California Institute of Technology.
[3] Austin J., Pintgen F. and Shepherd J.E. (2005). Proceedings of the Combustion Institute 30: 1849.
[4] Mével R. et al. (2014). International Journal of Hydrogen Energy 39:6044.
[5] Eder, A. (2001). Ph.D. thesis Technischen Universität München.
[6] Lee, S.-Y. et al. (2004). Journal of Propulsion and Power, Vol. 20, No 6, 1026:1036.
[7] Wang C., Xu S., and Fei L. (2007). Chinese Journal of Theoretical and Applied Mechanics 23:661.
[8] Bessler G. et al. (2003). Third Joint Meeting of the U.S. Sections of The Combustion Institute.
[9] Hanson, R. K. et al. (2015). Spectroscopy and optical diagnostics for gases, Springer.
[10] Gordon, I.E. et al. (2017). Journal of Quantitative Spectroscopy and Radiative Transfer 203, 3:69.
[11] Thiery, L. et al. (1996). Optics Communications 123, 801:809.
[12] Mével R. et al. (2009). Proceedings of The Combustion Institute 32:359.
[13] Mével R. et al. (2016). International Journal of Hydrogen Energy 41, 6905:6916.
[14] Shepherd J.E. (1986). Progress in Astronautics and Aeronautics 106, 263:293.
[15] Browne S., Ziegler J., and Shepherd J.E. (2006). GALCIT Report FM2006.006 - R3, California Institute of Technology, Revised September, 2018.
[16] Reynaud M., Virot F., and Chinnayya A. (2017). Physics of Fluids 29, (5), 056101.
[17] Savard B. et al. (2015). Journal of Computational Physics 29, (5), 740:769.